

# Integration of Biorecognition Elements on PEDOT Platforms through Supramolecular Interactions

Luciano D. Sappia, Esteban Piccinini, Waldemar Marmisollé, Natalia Santilli, Eliana Maza, Sergio Moya, Fernando Battaglini, Rossana E. Madrid, and Omar Azzaroni\*

The rapidly emerging field of organic bioelectronics exploits the functional versatility of conducting polymers to transduce biological recognition events into electronic signals. For the majority of biosensors or biomedical devices, immobilization of a biorecognition element is a critical step to improve the biotic/abiotic interface. In this work, a simple strategy is described to construct large-area all-plastic poly(3,4-ethylenedioxythiophene) (PEDOT) electrodes displaying carbohydrate biorecognizable motifs. First, the method involves the preparation of PEDOT-poly(allylamine) composites through supramolecular interactions. It is demonstrated by Raman and X-ray spectroscopy and cyclic voltammetry that the PEDOT:poly(allylamine) ratio and the film electroactivity can be easily controlled. Then, carbohydrate motifs are covalently anchored to the primary amine groups by a straightforward route using divinylsulfone chemistry. The recognition-driven assembly of the lectin concanavalin A (Con A) and the glycoenzyme glucose oxidase (GOx) onto mannosylated surfaces is demonstrated by surface plasmon resonance spectroscopy. Furthermore, the bioelectrocatalytic glucose detection mediated by the assembled enzyme is studied for all-plastic and gold electrodes. Interestingly, the synergistic combination of conducting polymers and recognition-directed assembly leads to a 2.7-fold enhancement of the bioelectrocatalytic signal. Finally, it is proved that Con A/GOx nanoarchitectures can be constructed onto PEDOT platforms using the layer-by-layer technique.

## 1. Introduction

Since the seminal work reported by Heeger and co-workers in 1977,<sup>[1]</sup> conducting polymers (CPs) have attracted much interest from academic and industrial researchers to explore their potential in bioelectronics, such as in biosensors, biomedical implants, and tissue engineering.<sup>[2–5]</sup> In particular, poly(3,4-ethylenedioxythiophene) (PEDOT) has emerged as a versatile CP used for biomedical and sensing applications.<sup>[4,6–10]</sup> The soft characteristics of this conducting polymer assures compatibility with flexible substrates,<sup>[11]</sup> and allows good mechanical matching with delicate biological systems.<sup>[12]</sup>


For the development of functional bioelectronic devices based on CPs, the incorporation of enzymes is especially important owing to their excellent functional properties, which include activity, selectivity, and specificity.<sup>[13,14]</sup> It should be noted that the biodevice performance is strongly dependent on the characteristics of the bio-/non-biointerfacial architecture

L. D. Sappia, N. Santilli, Prof. R. E. Madrid  
Laboratorio de Medios e Interfases  
Departamento de Bioingeniería  
Fac. de Cs. Exactas y Tecnología  
Universidad Nacional de Tucumán  
Av. Independencia 1800  
4000 San Miguel de Tucumán, Argentina

L. D. Sappia, Prof. R. E. Madrid  
Instituto Superior de Investigaciones Biológicas  
CONICET  
Chacabuco 461  
T4000ILI San Miguel de Tucumán, Argentina

E. Piccinini, Dr. W. Marmisollé, Prof. O. Azzaroni  
Instituto de Investigaciones Fisicoquímicas Teóricas y Aplicadas  
Departamento de Química  
Facultad de Ciencias Exactas  
Universidad Nacional de La Plata  
CONICET  
CC 16 Suc. 4, B1904AMD La Plata, Argentina  
E-mail: azzaroni@inifta.unlp.edu.ar

Dr. E. Maza, Prof. S. Moya  
Soft Matter Nanotechnology Group  
CIC biomaGUNE, Paseo Miramón 182  
20009 San Sebastián, Gipuzkoa, Spain  
Prof. F. Battaglini  
INQUIMAE  
Departamento de Química Inorgánica  
Analítica y Química Física  
Facultad de Ciencias Exactas y Naturales  
Universidad de Buenos Aires  
Ciudad Universitaria  
Pabellón 2, C1428EHA Buenos Aires, Argentina

 The ORCID identification number(s) for the author(s) of this article can be found under <https://doi.org/10.1002/admi.201700502>.

DOI: 10.1002/admi.201700502

and the characteristics of the association between the biomacromolecules and the surface.<sup>[15–19]</sup> For instance, covalent multipoint attachment of proteins is likely to disrupt the folding and the functionality of the native molecule if essential groups are involved in the binding process.<sup>[20,21]</sup> On the other hand, recognition-directed assembly emerged as an interesting and attractive alternative due to its simplicity and versatility, without introducing chemical modifications into the enzyme.<sup>[22]</sup> In this sense, increasing research efforts have been focused on the biorecognition-directed functionalization of CPs to enhance their biocompatibility, stability and functionality.<sup>[23–27]</sup>

The biofunctionalization of PEDOT can be achieved by the covalent or noncovalent anchoring of recognition elements to the polymer matrix.<sup>[28]</sup> The main reported approaches rely on the electropolymerization of EDOT derivatives containing the recognition motif, or a functional group that can be modified in a subsequent step with the recognition motif.<sup>[26,29–32]</sup> EDOT electropolymerization can also be done in the presence of biomacromolecules to entrap them into the conductive material.<sup>[23,33,34]</sup> Nevertheless, the introduced biological molecules could disrupt the electrical properties of the CP or lead to the loss of bioactivity post electropolymerization.<sup>[27]</sup> Another drawback of the electropolymerization technique is that it must be carried out on an electrically conducting substrate, e.g., Au, Pt, ITO, carbon paste. This can be an inconvenient when transparency and low cost production are required features of the devices.<sup>[11,35]</sup>

To overcome this issue, the chemical polymerization of EDOT using Fe<sup>(III)</sup> as an oxidant and tosylate (Tos) as a negative dopant represents a simple strategy to construct highly conductive all-plastic electrodes.<sup>[36–38]</sup> The synthetic route reported by Rozlosnik and co-workers allows for the deposition of large-area PEDOT:Tos films on plastic substrates by spin-coating. To achieve the goal of biofunctionalizing the conductive films, the chemical polymerization in the presence of an easily modifiable polymer (e.g., PSS-co-MA<sup>[39,40]</sup> and PVA<sup>[41]</sup>) is an attractive alternative. This leads to stable hybrid composites, where the added polymer is confined within the PEDOT matrix by supramolecular interactions. Subsequently, a recognition element can be covalently linked to the exogenous functional group: MA or PVA.

The choice of the recognition element of the bio/abiotic interface depends on the nature of the biomolecule that needs to be immobilized. Glycans can be employed as biofunctional ligands for the targeting of specific glycan binding proteins, i.e., lectins.<sup>[42,43]</sup> Moreover, it has been well reported that lectin-modified surfaces can be used for an efficient and rapid assembly of a considerable amount of glycoenzymes driven by bioaffinity interactions.<sup>[44,45]</sup> This is applicable to native proteins and is simply based on the supramolecular interactions that living systems use to form biomolecular complexes. Of particular interest, lectin-glycoenzyme supramolecular assemblies with remarkable stability are spontaneously formed driven by lectin-carbohydrate molecular recognition.<sup>[46,47]</sup>

Herein, we describe for the first time the synergistic combination of conducting polymers (CPs) and recognition-directed assembly to immobilize redox glycoenzymes on all-plastic conductive platforms and bioelectrocatalyze their substrate oxidation. First, PEDOT–poly(allylamine) (PEDOT–PAH) composites

were prepared under different PEDOT–PAH ratios by chemical polymerization of PEDOT using Fe<sup>(III)</sup> tosylate (Tos) in presence of PAH, and characterized by Raman, X-ray spectroscopy (XPS), and cyclic voltammetry. Special attention was paid to correlate the PEDOT electroactivity with the amount of PAH entrapped in the polymer matrix. The PAH amine groups were modified using the divinylsulfone (DVS) cross-linker to anchor carbohydrates to the composite surface. Then, the recognition events of concanavalin A (Con A) and glucose oxidase (GOx), a model lectin and glycoenzyme, to the glycosylated surface were explored by surface plasmon resonance (SPR) spectroscopy. Finally, the bioelectrocatalytic oxidation of glucose by means of the assembled redox enzyme was studied in detail. Our results reveal that not only the redox enzymes can be assembled onto all-plastic electrodes, but also the bioelectrocatalytic activity is higher when GOx is assembled on Con A-modified PEDOT–PAH platforms than on Con A-modified Au.

## 2. Results and Discussions

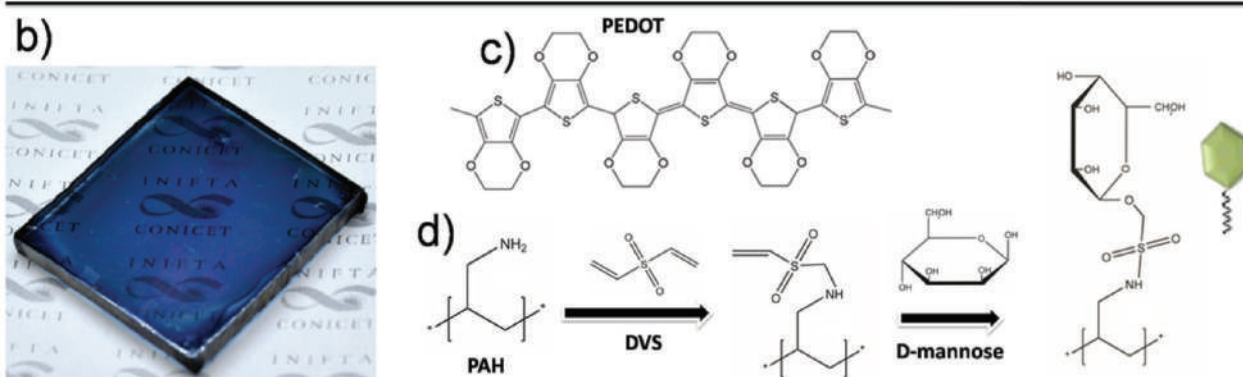
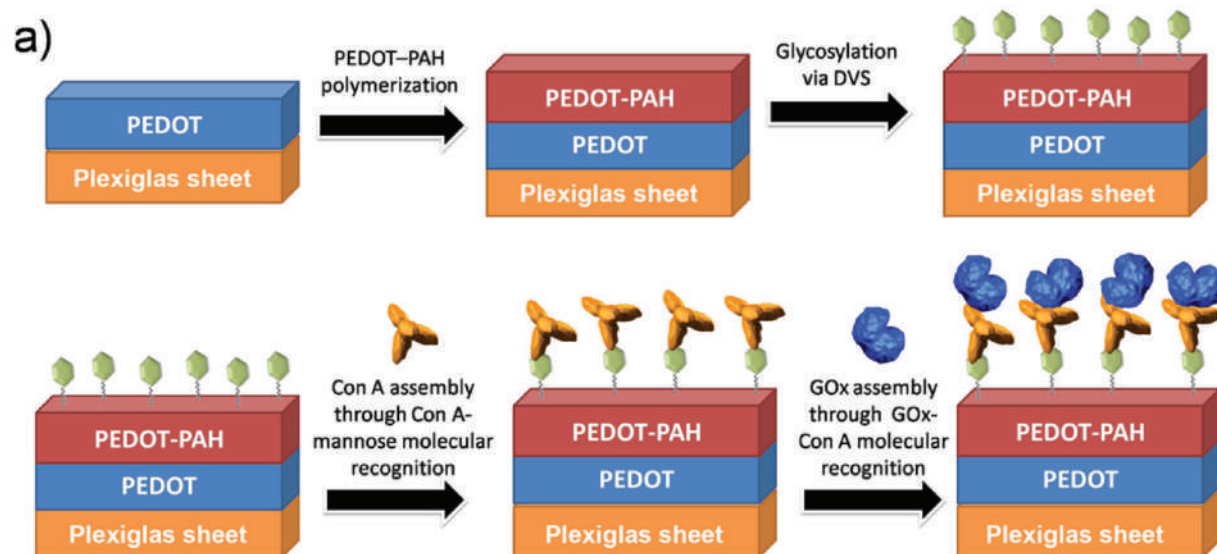
### 2.1. Amine-Terminated PEDOT Platforms: Synthesis and Characterization

The construction process of the all-plastic conductive platforms is described in the **Scheme 1a**. First, two layers of PEDOT were deposited on Plexiglas substrates by spin-coating. PEDOT films showed remarkable adhesion to the Plexiglas substrates. The thickness, measured by ellipsometry, of one PEDOT layer was 56 nm (data shown in the Supporting Information). For the preparation of the hybrid composites, a third layer of PEDOT–PAH<sub>x</sub> was deposited on the PEDOT films using different amount of PAH in the polymerization solution: 15 mg (PEDOT–PAH1), 40 mg (PEDOT–PAH2), and 75 mg (PEDOT–PAH3). **Scheme 1b** shows a photo of a PEDOT–PAH1 composite prepared on a Plexiglas substrate. Throughout this section, a detailed physicochemical and electrochemical characterization of the conductive hybrid films is reported.

#### 2.1.1. Raman Spectroscopy

The Raman spectrum for the pristine PEDOT layer, red line in **Figure 1a**, presents bands with a very good correlation with the literature:<sup>[48,49]</sup> the peak at 437 cm<sup>-1</sup> is assigned to SO<sub>2</sub> bending, 577 cm<sup>-1</sup> is related to oxyethylene ring deformation, 701 cm<sup>-1</sup> to symmetric C–S–C deformation, 989 cm<sup>-1</sup> is assigned to oxyethylene ring deformation, 1093 cm<sup>-1</sup> is the C–O–C deformation, 1255 cm<sup>-1</sup> is the C<sub>α</sub>–C<sub>α</sub> inter-ring stretching, 1365 cm<sup>-1</sup> to C<sub>β</sub>–C<sub>β</sub> stretching, 1421 cm<sup>-1</sup> to symmetric C<sub>α</sub>=C<sub>β</sub>(–O) stretching, and the 1563 cm<sup>-1</sup> peak is assigned to the asymmetric C<sub>α</sub>=C<sub>β</sub> stretching. The good correlation of the Raman spectra features with those reported elsewhere does prove the chemical state of the obtained PEDOT films.<sup>[48,49]</sup>

The Raman spectrum of the pristine PEDOT (brown line) can be compared with that of the PEDOT–PAH composite film (orange line), reported in **Figure 1a**. In general, all the peaks of the PEDOT Raman spectrum are also exhibited in the PAH–PEDOT composites, evidencing that the PEDOT



**Scheme 1.** a) Steps of the biosensor construction process: Deposition of two consecutive layers of pristine PEDOT on acrylic substrate, PEDOT–PAH deposition, mannosylation of the amine-terminated composite, assembly of Con A, and assembly of GOx. b) Image of an acrylic substrate with two layers of pristine PEDOT and a third layer of PEDOT–PAH1. c) PEDOT chemical structure. d) Divinylsulfone chemistry for the mannosylation of amine-terminated composites.

chemical structure is preserved. The main difference is in the region  $1450\text{--}1600\text{ cm}^{-1}$ . For assignment purposes, we have also prepared a substrate depositing PAH on a PEDOT film by drop-casting from an aqueous solution (PEDOT + PAH). From the analysis of the normalized spectra (inset), the changes in the peaks at about  $1500$  and  $1560\text{ cm}^{-1}$  in the hybrid films (PEDOT–PAH) as compared with PEDOT can be attributed to the presence of PAH within the films as they also appear in the PEDOT + PAH film. The broad bands in the region  $1500\text{--}1600\text{ cm}^{-1}$  could be attributed to bending modes of the polyamine as reported elsewhere for PAH.<sup>[50]</sup> The presence of the amine moieties in the composite films will be corroborated by XPS in the next section.

### 2.1.2. XPS of PEDOT–PAH Composites

In order to determine the content of PAH contained in the films as a function of the concentration of PAH in the polymerization solution, the PEDOT–PAH<sub>x</sub> composites were analyzed by XPS. Figure 1b shows the survey scans corresponding to

PEDOT and PEDOT–PAH<sub>x</sub> films prepared on glass substrates. There is a marked increase of the intensity in the N1s region by adding PAH to the hybrid PEDOT composites. Moreover, the incorporation of PAH led to a distortion of the S2p signal. Further analysis was done by studying the nitrogen and sulfur core regions in detail.

The XPS core regions of N1s and S2p for a particular film (PEDOT–PAH2) are presented in Figure 1c. The baseline corrected N1s core XPS signal can be quantitatively fitted by two bands at  $401.8\text{ eV}$  and  $399.7$  (full width at half maximum (FWHM)  $2.0\text{ eV}$ ).<sup>[51]</sup> These bands have been assigned to N–C species of protonated and neutral amines, respectively.<sup>[51]</sup> Therefore, from the integration of these two bands, the protonation degree of the PAH can be determined (Table 1).<sup>[50]</sup> These calculations reveal that the PAH incorporated to the films is mainly charged. The spectrums of the PEDOT–PAH1 and PEDOT–PAH3 samples are presented in Figure S4 (Supporting Information).

The XPS S2p core region can be satisfactorily fitted by two sets of doublets (FWHM  $1.9\text{ eV}$ ) at about  $165$  and  $169\text{ eV}$  corresponding to S atoms from PEDOT and from tosylate,

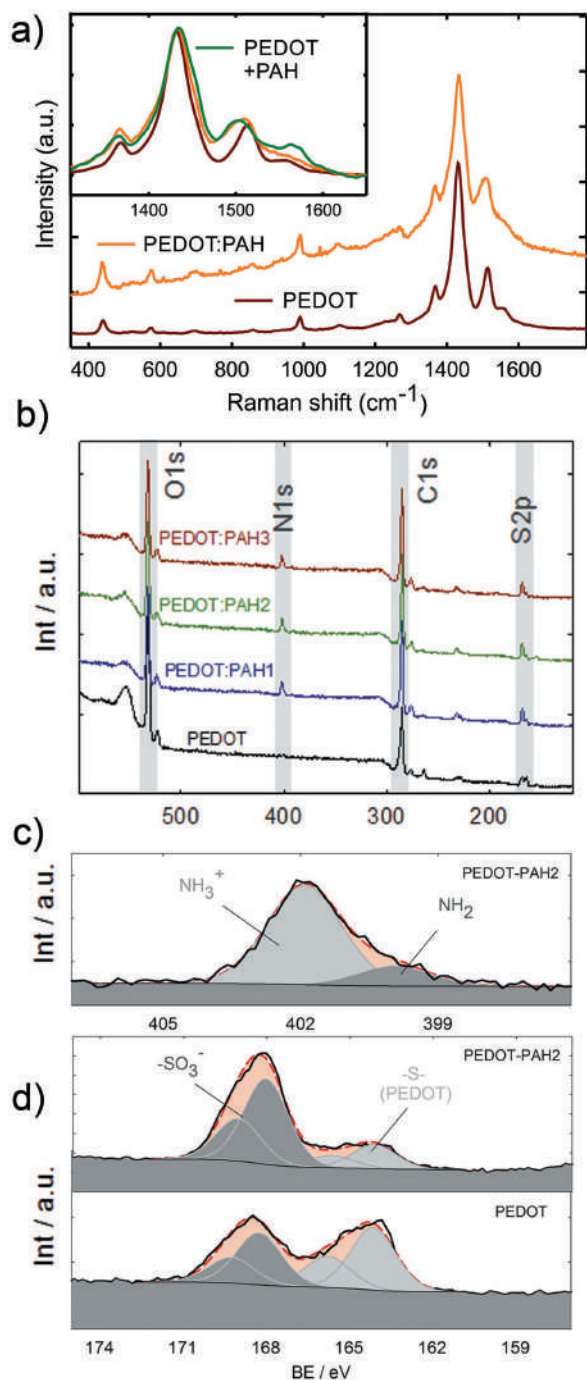


**Figure 1.** a) Raman spectra of two layers of pristine PEDOT film (red line) and the PEDOT–PAH composite (15 mg PAH, orange line). The marks correspond to the differences that were found between the samples. b) XPS survey spectra of PEDOT and PEDOT–PAH with different amount of PAH in the polymerization solution (PEDOT–PAH<sub>x</sub>). XPS detailed spectra of c) the N1s and d) the S2p core regions of a PEDOT–PAH2 film. The S2p spectrum of pristine PEDOT was added for comparison.

respectively,<sup>[86]</sup> as shown in Figure 1d. The higher binding energy doublet corresponds to sulfur signal (S2p) in the sulfonate group which appears at about 169 eV and can be fitted to a set of two bands at 169.2 and 168.1 eV, assigned to S2p1/2

and S2p3/2, respectively, with an integrated area ratio of 1:2 which takes into account the relative degeneration of these levels.<sup>[52]</sup> The same restriction was employed for fitting the signal attributed to sulfur in PEDOT backbone, which appears centered at 164.8 eV, as usually reported.<sup>[53,86]</sup> The bands of the doublet were fitted to be at 165.6 and 164.1 eV for the S2p1/2 and S2p3/2 components, respectively. As shown in Table 1, the proportion of sulfonate is higher when PAH is incorporated to the films. This is consistent with the incorporation of a great amount of positively charged groups, which demands a higher proportion of negative counterions within the films for charge compensation.

Quantitative determination of the total nitrogen to sulfur N/S atomic ratios was performed from the integrated intensity of the N1s and S2p core signals (see Table 1). The effective relative cross-section was determined by measuring a sample of (NH<sub>4</sub>)<sub>2</sub>S<sub>2</sub>O<sub>8</sub> powder in the same conditions as standard reference. As previously reported,<sup>[53]</sup> a little N1s signal could be detected for pristine PEDOT, and may be attributed to some remaining pyridine within the films. Interestingly, the increment of the PAH concentration in the polymerization solution resulted in a slight increase of the N/S ratio. When the N/S ratio is calculated using only the PEDOT component of the S2p core signal, then, the PAH/PEDOT monomer ratio ( $n_{\text{PAH}}/n_{\text{PEDOT}}$ ) can be obtained. Moreover, the polymer mass ratio ( $m_{\text{PAH}}/m_{\text{PEDOT}}$ ) could be determined from the monomer ratio and the molecular weights. This way to express the polymer ratio is interesting because of being representative of the polymer volume ratio. In particular,  $m_{\text{PAH}}/m_{\text{PEDOT}}$  varied from 1.34 for PEDOT–PAH1 to 1.70 for PEDOT–PAH3. It is important to point out that this strategy to integrate the polyelectrolyte within the PEDOT matrix allows for controlling the content of population of amino groups in a simple manner.

### 2.1.3. Electrochemistry

Cyclic voltammetry was used to assess the PEDOT electroactivity after the addition of PAH (a nonconductive polymer). For the PEDOT film (see Figure S3 in the Supporting Information), the reduction and oxidation peaks were observed at –330 and –150 mV versus Ag/AgCl, in agreement with the literature.<sup>[54]</sup> Voltammetric results indicate that the incorporation of PAH to the conductive matrix, does not alter the electroactivity but it causes a slight shift of the reduction and oxidation peaks to lower potentials.

Cyclic voltammetry was also performed in the presence of  $1 \times 10^{-3}$  M potassium ferro-/ferricyanide as a redox couple. **Figure 2a** depicts the electrochemical response of the all-plastic electrodes varying the amount of PAH in the composite. All the hybrid composites showed well defined peaks of the redox couple with a formal potential of 195 mV, even for the composite with highest amount of the nonconductive polymer (green line in Figure 2a). Increasing the amount of PAH within the films resulted in a small decrease in the anodic and cathodic current peaks ( $I_{\text{ap}}$  and  $I_{\text{cp}}$ ). For example,  $I_{\text{ap}}$  of the PEDOT–PAH2 (blue line) and PEDOT–PAH3 films are 2% and 11% lower than that for PEDOT–PAH1 (red line), see Table S1 in the Supporting Information for further details. Despite of being

**Table 1.** Components and relative composition determined from the fittings of the XPS results of the PEDOT and PEDOT–PAH<sub>x</sub> films (*m* = polymer mass).

Sample	S2p %S <sub>PEDOT</sub>	S2p %S <sub>SO<sub>3</sub><sup>-</sup></sub>	N1s % NH <sub>2</sub>	N1s % NH <sub>3</sub> <sup>+</sup>	N/S ratio	<i>m</i> <sub>PAH</sub> / <i>m</i> <sub>PEDOT</sub>
PEDOT	54.4	45.6	–	–	0.12	0
PEDOT–PAH1	25.4	74.6	15.5	84.5	0.87	1.34
PEDOT–PAH2	23.8	76.2	19.8	80.2	0.93	1.54
PEDOT–PAH3	22.1	77.9	16.9	83.1	0.95	1.70

a nonconductive polymer, the integration of PAH did not alter significantly the electroactivity of the PEDOT platform. The last observation was also confirmed by electrochemical impedance spectroscopy (EIS): no significant changes in the EIS response are caused by the introduction of the PAH within the PEDOT matrix (see the Supporting Information for more details). The hybrid composites were also measured at different scan rates in the presence of the ferro/ferricyanide redox couple (Figure 2b). A linear relation was obtained between the peak currents and

the square root of the scan rate (inset at Figure 2b), evidencing that the redox process was controlled by semi-infinite linear diffusion.<sup>[55]</sup> Moreover, the peak-to-peak separation between the anodic and the cathodic peak potential increased with the scan rate, which is characteristic of a quasi-reversible system.<sup>[56]</sup>

## 2.2. Recognition-Mediated Assembly of Concanavalin A and Glucose Oxidase to Glycosylated Surfaces

Once the presence of PAH in the PEDOT–PAH composites was confirmed by XPS and Raman techniques, we proceeded to the covalent anchoring of sugar motifs to the conductive all-plastic platform. To achieve this task, the divinylsulfone chemistry was exploited for the glycosylation of primary amines from the PAH integrated into the film. This straightforward synthetic route allows the attachment of D-mannose from aqueous solutions to surfaces containing nucleophilic groups, e.g. –OH, –NH<sub>2</sub>, and –SH.<sup>[57,58,84]</sup> In our work, the synthetic procedure reported by Hatakeyama et al.<sup>[84]</sup> was followed using the PEDOT–PAH films. The chemical process involves two sequential nucleophilic 1,4-additions (i.e., Michael addition) in alkaline solution at ambient temperature, wherein DVS serves as a linker between the nucleophilic group of surface and the nucleophilic group of the sugars (Scheme 1d). Cheng et al. demonstrated by N and C nuclear magnetic resonance that reducing sugars, like mannose; react via the most nucleophilic hydroxyl group, which is the –OH of the anomeric position. Of particular interest to this work, this reaction showed  $\alpha$  selectivity for the case of mannose.<sup>[57]</sup> That means that glycosylated surfaces exhibiting high specific recognition to Con A can be easily prepared. As demonstrated by other authors,<sup>[58]</sup> the success of the mannosylation via DVS can be proved measuring the wettability. A marked decrease in the contact angle (i.e., increase in hydrophilicity) was observed after the modification: from  $69.1^\circ \pm 0.5^\circ$  for a PEDOT–PAH1 film (top of Figure 3a) to  $25.3 \pm 1.7$  for a mannosylated PEDOT–PAH1 film (bottom of Figure 3a). The observed hydrophilicity increase after the covalent anchoring of the sugar motif is in agreement with previous reports,<sup>[58,59]</sup> and can be explained in terms of a large amount of sugar hydroxyl groups exposed on the surface. Further evidence of the chemical modification was obtained by XPS (see the Supporting Information). Importantly, the chemical modification approach did not impact on the resistance of the all-plastic films (Figure S10, Supporting Information).

Then, the construction of the lectin-glycoenzyme nanoarchitectures driven by molecular recognition on the mannosylated substrates was carried out. Surface plasmon resonance spectroscopy,<sup>[87]</sup> was chosen as a tool to assess in situ each assembly

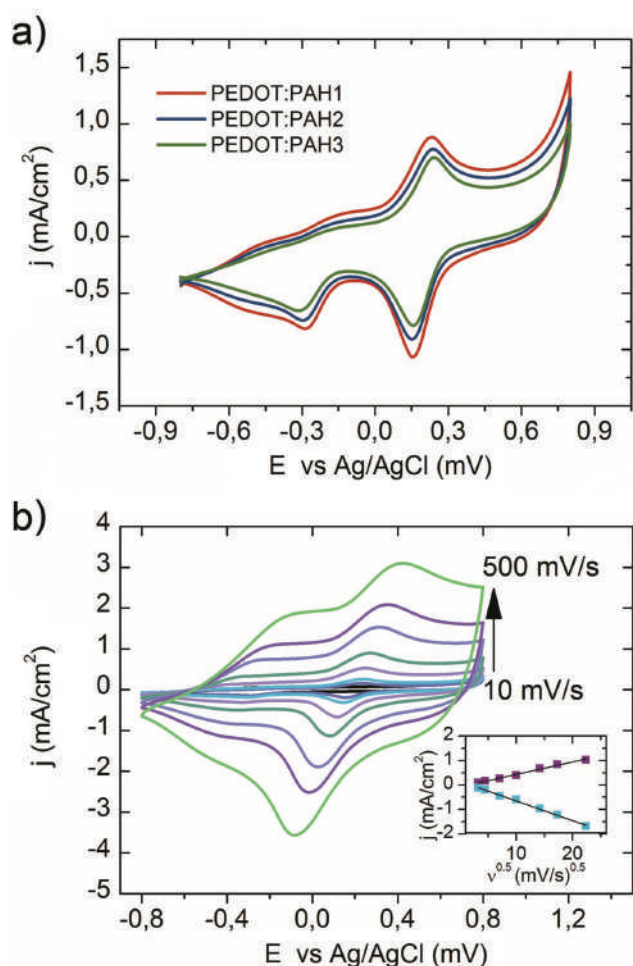


**Figure 2.** a) Cyclic voltammograms of PEDOT–PAH<sub>x</sub> composites in  $1 \times 10^{-3}$  M ferro/ferricyanide measured at  $50 \text{ mV s}^{-1}$ . b) Cyclic voltammograms of a PEDOT–PAH1 film in  $1 \times 10^{-3}$  M potassium ferro/ferricyanide measured at different scan rates (10, 20, 50, 100, 200, 300, and  $500 \text{ mV s}^{-1}$ ). Inset: Plot of the anodic and cathodic current peak as a function of the square-root of the scan rate.

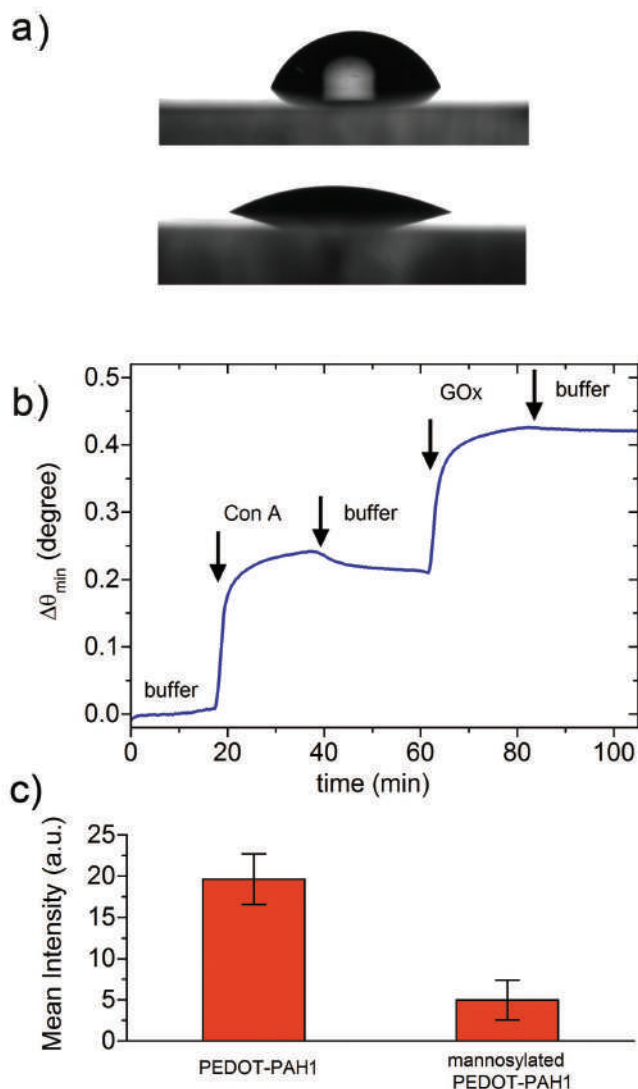


**Figure 3.** a) Contact angle images of PEDOT-PAH1 (top) and mannoseylated PEDOT-PAH1 (bottom) films using deionized water. b) Time-resolved SPR sensogram for the assembly of Con A and GOx on a mannoseylated gold sensor. The experiment was performed using a 785 nm laser and a flow rate of  $10 \mu\text{L min}^{-1}$ . c) Mean fluorescence intensity measured by fluorescence microscopy after the nonspecific adsorption of fluorescein-tagged BSA.

step. Since PEDOT films absorb UV-vis-NIR light and its dielectric constants depends strongly on the doped state,<sup>[60]</sup> measuring the assembly process of biomolecules on PEDOT films by SPR is not an easy task. To circumvent this issue, the assembly process was monitored using mannoseylated gold SPR substrates prepared with the same protocol as that for PEDOT-PAH films. Figure 3b depicts the change in the angle of minimum reflectance ( $\Delta\theta_{\min}$ ) of the Con A/GOx sequential assembly on mannoseylated gold sensors. The surface coverages ( $\Gamma$ ) were estimated by a comparison of  $\theta_{\min}$  before and after the incorporation of each protein. Surface coverage values for Con A and GOx assemblies were  $232 \text{ ng cm}^{-2}$  ( $2.23 \text{ pmol cm}^{-2}$ ) and  $225 \text{ ng cm}^{-2}$  ( $1.41 \text{ pmol cm}^{-2}$ ), respectively. Noticeably, the amount of Con A assembled on our mannoseylated

sensor (prepared by the DVS route) is higher than that reported using other mannoseylation route.<sup>[61,62]</sup> As explained in the next section, it is possible to estimate the  $\Gamma_{\text{GOx}}$  on the mannoseylated PEDOT-PAH platforms by a correlation between the SPR and the bioelectrochemical characterization. Concomitantly, atomic force microscopy characterization revealed that the consecutive assembly of Con A and GOx introduced some changes in the sample nanotopography (see Supporting Information for details).

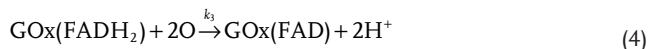
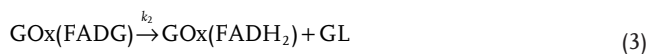
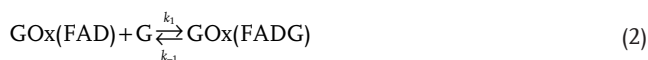
Although the sequential assembly of Con A and GOx was demonstrated to be effective and highly stable (see Figure S6 in the Supporting Information), the evaluation of the specificity is also important. For this purpose, the nonspecific adsorption of bovine serum albumin (BSA) onto the all-plastic platforms was compared prior to and after the mannoseylation step. Both platforms were incubated in a  $0.1 \text{ mg mL}^{-1}$  fluorescently tagged BSA (FITC-BSA) solution for 20 min and, then, rinsed with buffer. The mean fluorescence intensity was measured by fluorescence microscopy and is presented in Figure 3c (see the Supporting Information for the experimental details). Interestingly, the glycosylation of the PEDOT-PAH platform resulted in a significant decrease in nonspecific BSA adsorption. The mean intensity dropped almost four times, from 19 to 5. This observation, resulting from the exposure of carbohydrate motifs to the interface, is in full agreement with previous results reported by Prime and Whitesides.<sup>[63]</sup> According to these authors, nonspecific adsorption of proteins is prevented by surfaces displaying the following characteristics: have high hydrophilic character, hydrogen-bond acceptors, and overall electrical neutrality. In particular, glycosylated surfaces such as maltose-terminated<sup>[64]</sup> or galactose-terminated thiol monolayers<sup>[65]</sup> were reported as protein resistant substrates. Therefore, the glycosylation of the all-plastic platform plays two roles: (i) to allow the recognition-driven assembly of the lectin and (ii) to avoid the adsorption of proteins by nonspecific interactions.

While in this work we focused on the integration of carbohydrate motifs to recognize lectins and glycoproteins, it should be noted that the divinyl sulfone-activated PEDOT-PAH platforms could link other recognition elements such as DNA, peptides, and enzymes.<sup>[66]</sup> As a general rule, biomolecules containing  $-\text{OH}$ ,  $-\text{NH}_2$ , and  $-\text{SH}$  nucleophilic groups will be suitable.

### 2.3. Electrocatalysis of GOx Assembled on Con A-Modified PEDOT-PAH and Gold Electrodes

Once the redox enzyme is immobilized on the electrode surface, the biocatalysis of the substrate can be translated into an electrode process mediated by the electron transfer from a redox mediator to the prosthetic group of the enzyme. This electron-mediated bioelectrocatalytic reaction is one of the fundamental principles of “bioelectronics” with immediate implications in the design and development of biosensors.<sup>[67]</sup> If the bioelectrocatalytic features of redox enzyme-containing interfaces need to be studied, the cyclic voltammetry represents an excellent tool.<sup>[62,68]</sup> In this technique, the working electrode potential is scanned in the anodic direction to generate the oxidized form of the redox mediator (i.e., from ferrocenemethanol to ferroceniummethanol). Then, the oxidized redox mediator

triggers the catalytic process giving rise to a bioelectrochemical faradaic current. In the particular case of the glucose oxidation catalyzed by the redox-wired GOx, the bioelectrochemical process consists of the following sequence of reactions<sup>[69]</sup>



R and O are the reduced (ferrocenemethanol) and oxidized (ferroceniummethanol) forms of the mediator, respectively. FADH<sub>2</sub> is the reduced form of the flavin prosthetic group of the GOx and FAD corresponds to the oxidized form. FADG is the enzyme-substrate complex, G is β-D-glucose, and GL is glucono-δ-lactone.

Cyclic voltammograms in **Figure 4** depicts the bioelectrocatalytic glucose oxidation occurring at the Con A/GOx biointerfaces prepared onto a mannosylated gold surface (Figure 4a) and a mannosylated PEDOT-PAH film (Figure 4b). All the experiments were performed in the absence of O<sub>2</sub>, in the presence of 100 × 10<sup>-6</sup> M ferrocenemethanol as the redox mediator and at different concentrations of glucose. Without the addition of glucose (dotted line), the cyclic voltammograms of both studies reveal the typical diffusion-controlled behavior of a redox probe in solution. After the addition of glucose, the cyclic voltammograms showed an increase of the anodic peak current and a decrease of the cathodic peak current by means of the bioelectrocatalytic oxidation of β-D-glucose to glucono-δ-lactone.<sup>[68]</sup>

For each glucose concentration, the bioelectrocatalytic current contribution (*j<sub>cat</sub>*) can be obtained after subtraction of the redox mediator wave. The plots of the *j<sub>cat</sub>* as a function of the potential for Con A/GOx biointerfaces prepared on mannosylated gold and mannosylated PEDOT-PAH electrodes are presented in **Figure 5a**. A fast increase of *j<sub>cat</sub>* can be seen for both systems when the potential is closed to the ferrocenemethanol formal potential (*E*<sub>1/2 Au</sub> = 212 mV and *E*<sub>1/2 PEDOT-PAH</sub> = 227 mV vs Ag/AgCl). Moreover, when the concentration of the oxidized redox mediator in the electrode surface is maximum (i.e., *E* above 250 mV), then, *j<sub>cat</sub>* reaches a plateau. In this condition, the rate of the electrocatalyzed oxidation of glucose is as fast as possible. Despite of the ferrocenemethanol electrochemistry using PEDOT-PAH electrodes was not strictly Nernstian, the characteristics of the bioelectrocatalytic response was similar to that of gold electrodes (see Figure S7 in the Supporting Information). There were two little differences: *j<sub>cat</sub>* was shifted to higher potential values (consistent with the change of *E*<sub>1/2</sub>) and the slope of *j<sub>cat</sub>* as a function of *E* was not as high as in the gold electrodes (due to the quasi-reversibility). To obtain the glucose calibration plot, the catalytic current density at 350 mV was plotted against the glucose concentration (Figure 5b). Interestingly, the bioelectrocatalysis of the Con A/GOx assembly prepared on the all-plastic platform (red circles) was higher than prepared on the gold surface (blue circles).

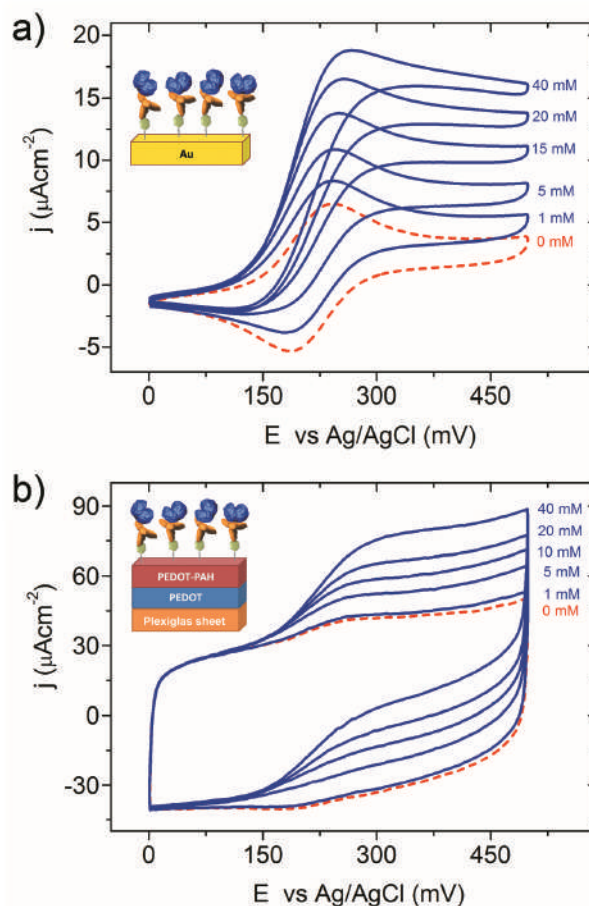


**Figure 4.** Cyclic voltammograms describing the bioelectrocatalysis of glucose oxidation occurring at Con A/GOx biointerfaces on a) a mannosylated gold electrode and b) a mannosylated PEDOT-PAH all-plastic electrode. [ferrocenemethanol] = 100 × 10<sup>-6</sup> M, *v* = 5 mV s<sup>-1</sup>, glucose concentrations indicated in each plot.

The theoretical formalism which describes the kinetic of the bioelectrochemical process was developed and demonstrated by Saveant and co-workers.<sup>[68,70]</sup> This formalism considers that the enzyme is immobilized on the electrode surface so as to form a monolayer (or a few layers) and the cosubstrate (ferrocenemethanol) diffuses from the solution to the electrode. In that case, the catalytic current density can be expressed as follows<sup>[68]</sup>

$$\frac{1}{j_{\text{cat}}} = \frac{1}{2F\Gamma_{\text{GOx}}} \left( \frac{1}{k_3[\text{O}]_{x=0}} + \frac{1}{k_2} + \frac{1}{k_{\text{red}}[\text{G}]} \right) \quad (5)$$

where  $k_{\text{red}} = k_1 k_2 / (k_{-1} + k_2)$ ,  $\Gamma_{\text{GOx}}$  is the GOx surface coverage, *j<sub>cat</sub>* is the bioelectrocatalytic current contribution, [G] is the glucose concentration in solution, [O]<sub>x=0</sub> is the concentration of ferrocenium in the surface of the electrode, and *F* is the Faraday constant.

It is important to note that the values of the kinetic constants involved in Equation (5) are only dependent on the redox mediator and the GOx catalytic activity. As we performed the bioelectrocatalytic experiments for GOx assembled on both

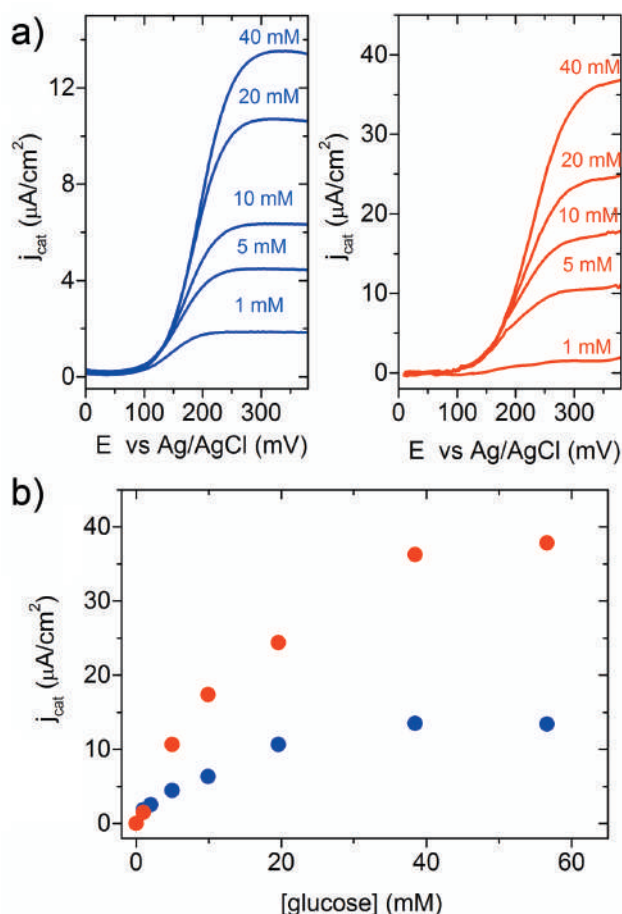


**Figure 5.** a) Bioelectrocatalytic component ( $j_{\text{cat}}$ ) of voltammetric data in Figure 4 corresponding to the assembly of Con A-GOx on mannosylated gold (left) and mannosylated PEDOT-PAH1 (right). b) Variation of the bioelectrocatalytic current density as a function of the substrate concentration for Con A-GOx assembled on mannosylated Au (blue) and mannosylated PEDOT-PAH1 (red).

platforms (i.e., mannosylated Au and mannosylated PEDOT-PAH) using the same redox mediator and the same immobilization approach, it may be considered that the values of the kinetic constants are the same for both systems. Moreover, when  $[O]_{x=0}$  reaches its maximum value, i.e., when  $j_{\text{cat}}$  reached the plateau and  $[G]$  is above the saturation concentration, then,  $j_{\text{cat}}$  is only dependent on  $\Gamma_{\text{GOx}}$  (see Equation (5)). Since the  $\Gamma_{\text{GOx}}$  for mannosylated Au was determined by SPR, the  $\Gamma_{\text{GOx}}$  for mannosylated PEDOT-PAH can be estimated by a direct comparison of  $j_{\text{cat}}$ . At  $40 \times 10^{-3}$  M glucose,  $j_{\text{cat}}$  of the biosensors prepared on Au and PEDOT-PAH was 13.5 and 36.2  $\mu\text{A cm}^{-2}$ , respectively. Because of the  $\Gamma_{\text{GOx}}$  on the Con A modified Au was 1.41  $\text{pmol cm}^{-2}$ , the obtained  $\Gamma_{\text{GOx}}$  on the Con A-modified PEDOT-PAH was 3.78  $\text{pmol cm}^{-2}$ . This value is almost one order of magnitude higher than that reported by Piro et al. for GOx covalently attached to polyethylenglycol and then entrapped in a PEDOT film.<sup>[71]</sup> Noticeably, the amount of GOx on the PEDOT-PAH platform was 2.7 times higher than that obtained for the Au platform. This result may be explained in two ways: the increase in the protein surface coverage was due to a roughness increase (i.e., larger effective area) of the PEDOT-PAH composites as

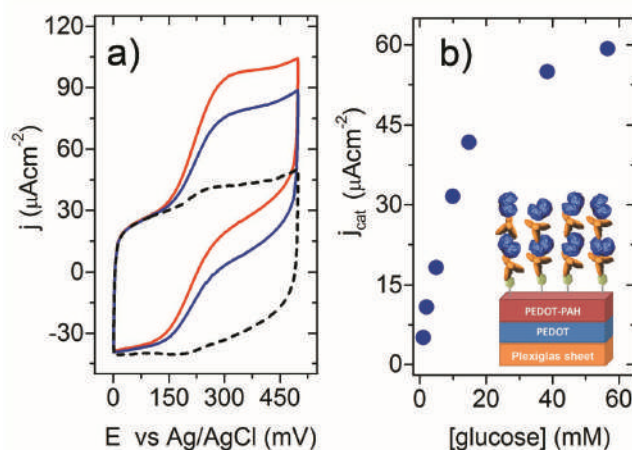


**Figure 6.** a) Cyclic voltammograms in the absence (dashed line) and in the presence of  $40 \times 10^{-3}$  M glucose (solid lines) for  $(\text{Con A}/\text{GOx})_1$  (blue line) and  $(\text{Con A}/\text{GOx})_2$  (red line) assemblies on mannosylated PEDOT-PAH1 electrodes. b) Glucose calibration plot for  $(\text{Con A}/\text{GOx})_2$  on mannosylated PEDOT-PAH1. The experiments were performed using ferrocenemethanol ( $100 \times 10^{-6}$  M) as a redox mediator.  $\nu = 5 \text{ mV s}^{-1}$ .

compared with gold surfaces.<sup>[72]</sup> On the other hand, considering the soft characteristics of the mannosylated PEDOT-PAH composites, the polymer-liquid interface could reorganize to uptake a larger amount of proteins.

The design of biofunctional interfaces with controllable activity is a major goal in bioelectronic devices. In our system, this is nontrivial task because only the redox enzymes which are close enough (in the nanoscale range) to the electrode surface will be efficiently wired.<sup>[68]</sup> With this purpose in mind, the layer-by-layer assembly technique can be used to increase the amount of loaded enzyme with nanoscale precision within the film.<sup>[62,73]</sup> By means of this technique, the lectin Con A can be employed as a supramolecular cross-linker of glycoproteins.<sup>[46]</sup> Figure 6a depicts the bioelectrocatalysis of Con A/GOx assemblies containing one (blue line) and two (red line) bilayers on the mannosylated PEDOT-PAH films in the presence of  $40 \times 10^{-3}$  M glucose. As expected, the  $(\text{Con A}/\text{GOx})_2$  assembly showed higher anodic current density as compared to  $(\text{Con A}/\text{GOx})_1$ , due to higher amount of enzyme and the concomitant increment of the catalyzed glucose oxidation (see Figures 5b and 6b above the saturation concentration of glucose). The electrochemically obtained  $\Gamma_{\text{GOx}}$  for the  $(\text{Con A}/\text{GOx})_2$  assembly was 5.90  $\text{pmol cm}^{-2}$ . Therefore, these results evidence two facts: the assembly of a second bilayer increased the amount of GOx on the conductive platform, and the adsorbed GOx was electrochemically connected to the PEDOT-PAH platform. Moreover, the  $(\text{Con A}/\text{GOx})_2$  all-plastic platform exhibited a linear range up to  $15 \times 10^{-3}$  M, a sensitivity of  $3.02 \pm 0.16 \mu\text{A cm}^{-2} \text{ mM}^{-1}$  (Figure S8, Supporting Information) and a LOD of  $0.16 \times 10^{-3}$  M. Even though these devices were constructed on Plexiglas (a nonconductive material), the obtained sensing features (LOD and sensitivity) are comparable with other PEDOT-based glucose sensors prepared on conductive substrates such as Au,<sup>[74]</sup> Pt,<sup>[75,76]</sup> graphite,<sup>[71,77,78]</sup> and ITO.<sup>[79]</sup>



### 3. Conclusion

In summary, we have presented a simple strategy to construct large-area all-plastic electrodes with biorecognizable motifs. To the best of our knowledge, this interfacial architecture represents the first report of biorecognizable all-plastic platforms capable of spontaneously assembling glycoenzymes and electrochemically “wire” their redox-active prosthetic groups to the electrode surface by the use of a redox mediator in solution. The method involves the integration of PAH within the PEDOT matrix. By varying the amount of PAH in the polymerization solution, the PEDOT–PAH ratio and the film electroactivity can be controlled. Then, mannose motifs were covalently anchored to the primary amine groups by a straightforward  $\alpha$ -anomer-selective synthetic route using the cross-linker divinylsulfone. By the use of SPR, we demonstrated that lectin-glycoenzyme assemblies driven by lectin-carbohydrate recognition can be effectively constructed onto the mannosylated electrodes. Moreover, the bioelectrocatalytic oxidation of glucose by means of the assembled redox enzyme was studied for all-plastic electrodes and compared to gold electrodes. Interestingly, the synergistic combination of conducting polymers and recognition-directed assembly led to a 2.7-fold enhancement of the bioelectrocatalytic signal. It is important to highlight that, even though these devices were constructed on a nonconductive material, the obtained sensing features are comparable to other PEDOT-based glucose sensors prepared on conductive substrates such as Au, Pt, and ITO. We believe that this approach for the construction of glycosylated all-plastic electrodes could have profound implications in the fields of biosensing and tissue engineering. For instance, bacterial cell walls expose a glycan layer that could be biorecognized by lectins,<sup>[80]</sup> thus we envision an alternative biosupramolecular method to assemble bacterial cells to all-plastic electrodes for diagnosis of bacterial infections with disposable devices. On the other hand, it was reported that neuron-silicon junctions can be created by attaching cells to the substrate by using Con A as a supramolecular linker. In a similar way, glycosylated conducting polymers modified with Con A could expand the frontiers of bioelectronics, for example, by interfacing neurons and organic field-effect transistors.<sup>[81]</sup>

### 4. Experimental Section

**Construction of PEDOT–PAH Films on Plexiglas Substrates:** PEDOT films were prepared by in situ polymerization of EDOT monomer solutions spin-coated on Plexiglas sheets and glass substrates, respectively. Previous to the polymerization, substrates were cleaned with ethanol, MilliQ water and dried. First, the oxidant solution was prepared mixing 715  $\mu\text{L}$  of 40%  $\text{Fe}(\text{III})$  tosylate butanol solution (CB 40, Clevios) 220  $\mu\text{L}$  of butanol (ACS, Merck) and 16.5  $\mu\text{L}$  of pyridine (ACS, Biopack).<sup>[36]</sup> Then, 915  $\mu\text{L}$  of the oxidant solution was mixed with 12.5  $\mu\text{L}$  of the EDOT monomer (97%, Sigma-Aldrich). This solution was homogenized in a vortex and filtered (pore diameter: 0.2  $\mu\text{m}$ ). The deposition was immediately carried out by spin-coating (WS-650MZ-23NPP, Laurell) using the resultant mixture at 1000 rpm for 1 min and an acceleration of 500 rpm  $\text{min}^{-1}$ . Then, in order to evaporate the pyridine that is used as an inhibitor of the polymerization, the substrates were heated at 70  $^{\circ}\text{C}$  for 15 min.<sup>[82,83]</sup> The color of the film changes from brown to green (Figure S1, Supporting Information). The green color is characteristic of the  $\text{Fe}^{3+}$  ions present in the dopant solution. Films were

immersed in deionized water for 5 min, then rinsed again with water and dried with  $\text{N}_2$  gas.

Polyallylamine hydrochloride (PAH) ( $M_w = 58$  kDa, Sigma-Aldrich) was incorporated into the PEDOT structure to provide a building block bearing amine groups. Different PEDOT–PAH composites were prepared varying the amount of PAH in the polymerization solution: PEDOT–PAH1 (15 mg), PEDOT–PAH2 (40 mg), and PEDOT–PAH3 (75 mg). First, the PAH was dissolved in 200  $\mu\text{L}$  of MilliQ water. Second, 915  $\mu\text{L}$  of the oxidant solution was added to each PAH solution and mixed vigorously. Finally, the EDOT monomer was added to the polymerization solution, and the resultant solution was filtered and deposited on the substrates by spin-coating.

**Glycosylation of Amino Terminated PEDOT–PAH Composites:** The glycosylation of the primary amines from the hybrid films was carried out following the protocol reported by Hatakeyama et al.<sup>[84]</sup> First, the PEDOT–PAH films were incubated in a 5% divinylsulfone (V3700, Sigma-Aldrich) carbonate buffer solution ( $\text{Na}_2\text{CO}_3$  0.5 M, pH 11 adjusted with HCl 0.5 N) for 1 h, and washed with carbonate buffer. After that, the substrates were immersed in a 10% wt mannose (112585, Sigma-Aldrich) carbonate buffer solution for 18 h. All the incubations were performed at room temperature. Finally, the electrodes were rinsed thoroughly with Tris buffer (Tris  $10 \times 10^{-3}$  M, NaCl 0.1 M pH = 7.5) and stored at 4  $^{\circ}\text{C}$  until they were used. Chemical reactions involved in the PEDOT–PAH mannosylation are described in Scheme 1d.

**Gold Substrates Functionalization for Electrochemical and SPR Measurements:** Basic piranha solution ( $\text{H}_2\text{O}_2$  30% and  $\text{NH}_4\text{OH}$  35% 1:1) was used to clean gold SPR substrates (SPR102 AU, BioNavis) at 60  $^{\circ}\text{C}$  for 10 min. A self-assembled monolayer was prepared by incubation of the Au sensors in a  $5 \times 10^{-3}$  M cysteamine (153/70050, Acros organics) (absolute) ethanol solution for 4 h. The sensors were washed with ethanol and dried with  $\text{N}_2$ . Then, the amine-terminated Au surfaces were glycosylated with the same protocol as the PEDOT–PAH films.

**Glycoprotein Assembly Mediated by Molecular Recognition:** The recognition-driven assembly of ConA and GOx on mannosylated surfaces was carried out as previously reported.<sup>[43]</sup> Mannosylated gold and PEDOT–PAH substrates were incubated for 30 min in a  $1 \times 10^{-6}$  M concanavalin A ( $M_w = 104$  kDa, C2010, Sigma-Aldrich) solution containing  $20 \times 10^{-3}$  M HEPES,  $0.5 \times 10^{-3}$  M  $\text{CaCl}_2$ , and  $\text{MnCl}_2$  at pH 7.4. The buffer was supplemented with  $\text{Ca}^{+2}$  and  $\text{Mn}^{+2}$  to promote the lectin-carbohydrate recognition.<sup>[85]</sup> After the concanavalin A modification, the platforms were rinsed with HEPES buffer, and then immersed in a  $1 \times 10^{-6}$  M glucose oxidase ( $M_w$  of 160 kDa, IMU, Aspergillus niger, 225 U  $\text{mg}^{-1}$ , Calzyme, USA) solution containing HEPES,  $\text{Ca}^{+2}$  and  $\text{Mn}^{+2}$ . The Con A/GOx multilayer assemblies were prepared by repeating the incubations as a cycle.

**Raman Spectroscopy:** Raman spectra were acquired using an i-Raman BW415-532S (BWTek) Raman spectrometer. The excitation wavelength was 532 nm and the laser was focused on the substrates by a 20 $\times$  optical microscope (BAC151B, BWTek). The operative power on the samples was 10 mW. The spectral region analyzed ranged from 100 to 4000  $\text{cm}^{-1}$ . The polymer samples were prepared on Au substrates to avoid the intense background signal that was observed in the case of the acrylic substrates.

**X-Ray Photoelectron Spectroscopy (XPS):** XPS was performed using a SPECS SAGE HR 100 system spectrometer. A Mg K $\alpha$  (1253.6 eV) X-ray source was employed operating at 12.5 kV and 10 mA. The take-off angle was 90 $^{\circ}$  and operating pressure was  $8 \times 10^{-8}$  mbar. Quantitative analysis of spectra was carried out by using the Casa XPS software, employing Shirley baselines and Gaussian/Lorentzian (30%) product functions. Surface-charging effects were corrected by setting the binding energy of the main component of the core level C1s at 285 eV.<sup>[86]</sup> The FWHM was kept fixed for different components of a given element. For quantitative N/S (nitrogen/sulfur ratio) determinations, calculations were performed by recording the XPS spectrum of  $(\text{NH}_4)_2\text{S}_2\text{O}_8$  (Sigma-Aldrich) powder in the same conditions as internal reference. To measure XPS, the polymer samples were prepared on glass substrates.

**SPR Spectroscopy:** Molecular assemblies of Con A and GOx on mannosylated gold surfaces were monitored by SPR (BioNavis 210A)

spectroscopy using the Kretschmann configuration, with a 785 nm laser and a flow rate of 10  $\mu\text{L min}^{-1}$ . To estimate the surface coverage of the biocomponents, the SPR angle of minimum reflectivity,  $\theta_{\text{min}}$ , was measured in situ during the recognition-driven assembly. Then, the shift in the angle of minimum reflectivity ( $\Delta\theta$ ) was converted into mass surface coverage ( $\Gamma$ ,  $\text{ng cm}^{-2}$ ), using the following equation<sup>[87]</sup>

$$\Gamma = \frac{\Delta\theta kd}{d\eta/dC} \quad (6)$$

where  $kd$  is a SPR substrate dependent parameter, in this case provided by BioNavis, with a value of  $1.9 \times 10^{-7} \text{ cm deg}^{-1}$ . The refractive index increment ( $d\eta/dC$ ) of a high GOx coverage layer was obtained from literature with a value of  $1.77 \times 10^{-10} \text{ cm}^3 \text{ ng}^{-1}$ ,<sup>[88]</sup> and the refractive index increment of the assembled Con A were considered equal to that of GOx.<sup>[89]</sup> Con A and GOx molecular weights (104 and 160 kDa, respectively) were used to convert the total mass surface coverage to molar surface coverage.

**Electrochemical Measurements:** Cyclic voltammetry experiments were performed with a TEQ-03 potentiostat using a three-electrode cell (Figure S2, Supporting Information) equipped with: an Ag/AgCl (3 M NaCl) reference electrode, a platinum mesh counter electrode and the working electrode (fixed working electrode area of 0.18  $\text{cm}^2$ ). For the construction of the all-plastic PEDOT–PAH working electrodes, two layers of pristine PEDOT and then a third layer of PEDOT–PAH were deposited on the acrylic substrate.  $100 \times 10^{-6} \text{ M}$  ferrocenemethanol (Sigma-Aldrich) was used as redox mediator in 0.02 M pH 7.4 HEPES buffer and 0.1 M KCl as supporting electrolyte.  $\text{N}_2$  bubbling was used to remove dissolved oxygen from the glucose solutions for at least 30 min before using, and for 10 min between successive measurements. To reach the glucose mutarotation equilibrium state, stock 1 M glucose solution was prepared in HEPES buffer 24 h before the measurements.<sup>[90]</sup>

**Contact Angle Measurements:** Contact angles were measured using a Ramé–Hart contact angle system (Model 290) at 25  $^\circ\text{C}$ . In each measurement, a 1  $\mu\text{L}$  droplet of MilliQ water was dispensed onto the modified surface. The average contact angle value was obtained at five different positions of the same sample.

## Supporting Information

Supporting Information is available from the Wiley Online Library or from the author.

## Acknowledgements

L.D.S. and E.P. contributed equally to this work. This work was supported by the CONICET, ANPCyT (PICT-2010-2554 and PICT-2013-0905), the Austrian Institute of Technology GmbH (AIT – CONICET Partner Group: “Exploratory Research for Advanced Technologies in Supramolecular Materials Science” – Exp. 4947/11). L.D.S. and E.P. gratefully acknowledge the CONICET for the scholarships. R.E.M., W.M., and O.A. are staff researchers of CONICET. L.D.S. acknowledges Prof. Noemi Rozlosnik for her support and the practical training at the DTU Nanotech group, and Prof. R. M. S. Alvarez for Raman spectra analysis. E.M. and R.E.M. thank FP7-PEOPLE-HIGRAPHEN (Project No. 612704) for financial support. The authors thank Tomás Piccinini and Dr. Lorena Cortez for technical assistance and helpful discussions.

## Conflict of Interest

The authors declare no conflict of interest.

## Keywords

bioelectrochemistry, biosensing, glucose oxidase, molecular recognition, PEDOT

Received: May 1, 2017  
Revised: May 19, 2017  
Published online: July 10, 2017

- [1] S. Hideki, E. J. Louis, A. G. Macdiarmid, C. K. Chiang, A. J. Heeger, *Chem. Commun.* **1977**, 578.
- [2] A. J. Heeger, *Angew. Chem., Int. Ed. Engl.* **2001**, *40*, 2591.
- [3] H. E. Katz, J. Huang, *Annu. Rev. Mater. Res.* **2009**, *39*, 71.
- [4] G. Kaur, R. Adhikari, P. Cass, M. Bown, P. Gunatillake, *RSC Adv.* **2015**, *5*, 37553.
- [5] G. Ćirić-Marjanović, *Synth. Met.* **2013**, *177*, 1.
- [6] J. T. Mabeck, G. G. Malliaras, *Anal. Bioanal. Chem.* **2005**, *384*, 343.
- [7] N. Y. Shim, D. A. Bernards, D. J. Macaya, J. A. DeFranco, M. Nikolou, R. M. Owens, G. G. Malliaras, *Sensors* **2009**, *9*, 9896.
- [8] D. A. Bernards, D. J. Macaya, M. Nikolou, J. A. DeFranco, S. Takamatsu, G. G. Malliaras, *J. Mater. Chem.* **2008**, *18*, 116.
- [9] Z.-T. Zhu, J. T. Mabeck, C. Zhu, N. C. Cady, C. A. Batt, G. G. Malliaras, *Chem. Commun.* **2004**, 1556.
- [10] I. Gualandi, M. Marzocchi, E. Scavetta, M. Calienni, A. Bonfiglio, B. Fraboni, *J. Mater. Chem. B* **2015**, *3*, 6753.
- [11] N. Kim, H. Kang, J. H. Lee, S. Kee, S. H. Lee, K. Lee, *Adv. Mater.* **2015**, *27*, 2317.
- [12] R. M. Owens, G. G. Malliaras, *MRS Bull.* **2010**, *35*, 449.
- [13] N. Rozlosnik, *Anal. Bioanal. Chem.* **2009**, *395*, 637.
- [14] E. Battista, V. Lettera, M. Villani, D. Calestani, F. Gentile, P. A. Netti, S. Iannotta, A. Zappettini, N. Coppedè, *Org. Electron.* **2017**, *40*, 51.
- [15] F. Wei, W. Liao, Z. Xu, Y. Yang, D. T. Wong, C. M. Ho, *Small* **2009**, *5*, 1784.
- [16] I. Willner, B. Willner, *Trends Biotechnol.* **2001**, *19*, 222.
- [17] E. Katz, I. Willner, *Angew. Chem., Int. Ed. Engl.* **2004**, *43*, 6042.
- [18] V. Pardo-Yissar, E. Katz, I. Willner, A. B. Kotlyar, C. Sanders, H. Lill, *Faraday Discuss.* **2000**, *116*, 119.
- [19] R. Baron, B. Willner, I. Willner, *Chem. Commun.* **2007**, 323.
- [20] R. A. Sheldon, S. van Pelt, *Chem. Soc. Rev.* **2013**, *42*, 6223.
- [21] W. Scouten, J. Luong, R. Stephenbrown, *Trends Biotechnol.* **1995**, *13*, 178.
- [22] M. Sarikaya, C. Tamerler, A. K.-Y. Jen, K. Schulten, F. Baneyx, *Nat. Mater.* **2003**, *2*, 577.
- [23] J. A. Arter, D. K. Taggart, T. M. McIntire, R. M. Penner, G. A. Weiss, *Nano Lett.* **2010**, *10*, 4858.
- [24] G. Lautner, J. Kaev, J. Reut, A. Öpik, J. Rappich, V. Syritskii, R. E. Gyurcsányi, *Adv. Funct. Mater.* **2011**, *21*, 591.
- [25] K. Mohan, K. C. Donovan, J. A. Arter, R. M. Penner, G. A. Weiss, *J. Am. Chem. Soc.* **2013**, *135*, 7761.
- [26] T. Galán, B. Prieto-Simón, M. Alvira, R. Eritja, G. Götz, P. Bäuerle, J. Samitier, *Biosens. Bioelectron.* **2015**, *74*, 751.
- [27] X. Strakosas, B. Wei, C. Martin, R. M. Owens, B. Wei, *J. Mater. Chem. B* **2016**, *4*, 4952.
- [28] Z. Guo, H. Liu, C. Jiang, Y. Zhu, M. Wan, L. Dai, L. Jiang, *Small* **2014**, *10*, 2087.
- [29] R. B. Bazaco, R. Gómez, C. Seoane, P. Bäuerle, J. L. Segura, *Tetrahedron Lett.* **2009**, *50*, 4154.
- [30] L. Dong, B. Lu, X. Duan, J. Xu, D. Hu, K. Zhang, X. Zhu, H. Sun, S. Ming, Z. Wang, S. Zhen, *J. Polym. Sci., Part A: Polym. Chem.* **2015**, *53*, 2238.
- [31] F. Mouffouk, S. J. Higgins, *Electrochem. Commun.* **2006**, *8*, 15.
- [32] L. K. Povlich, J. C. Cho, M. K. Leach, J. M. Corey, J. Kim, D. C. Martin, *Biochim. Biophys. Acta, Gen. Subj.* **2013**, *1830*, 4288.

- [33] J. Bognár, J. Szucs, Z. Dorkó, V. Horváth, R. E. Gyurcsányi, *Adv. Funct. Mater.* **2013**, 23, 4703.
- [34] A. Menaker, V. Syritski, J. Reut, A. Öpik, V. Horváth, R. E. Gyurcsányi, *Adv. Mater.* **2009**, 21, 2271.
- [35] W. Meng, R. Ge, Z. Li, J. Tong, T. Liu, Q. Zhao, S. Xiong, F. Jiang, L. Mao, Y. Zhou, *ACS Appl. Mater. Interfaces* **2015**, 7, 14089.
- [36] J. Daprà, L. H. Lauridsen, A. T. Nielsen, N. Rozlosnik, *Biosens. Bioelectron.* **2013**, 43, 315.
- [37] K. Kiilerich-Pedersen, J. Daprà, S. Cherré, N. Rozlosnik, *Biosens. Bioelectron.* **2013**, 49, 374.
- [38] K. B. Andersen, N. O. Christiansen, J. Castillo-León, N. Rozlosnik, W. E. Svendsen, *Org. Electron.: Phys. Mater. Appl.* **2013**, 14, 1370.
- [39] J. E. Collazos-Castro, G. R. Hernández-Labrado, J. L. Polo, C. García-Rama, *Biomaterials* **2013**, 34, 3603.
- [40] H. Vara, J. E. Collazos-Castro, *ACS Appl. Mater. Interfaces* **2015**, 7, 27016.
- [41] X. Strakosas, M. Sessolo, A. Hama, J. Rivnay, E. Stavrinidou, G. G. Malliaras, R. M. Owens, *J. Mater. Chem. B* **2014**, 2, 2537.
- [42] N. C. Reichardt, M. Martín-Lomas, S. Penadés, *Chem. Soc. Rev.* **2013**, 42, 4358.
- [43] D. Pallarola, N. Queralto, F. Battaglini, O. Azzaroni, *Phys. Chem. Chem. Phys.* **2010**, 12, 8071.
- [44] T. Hoshi, S. Akase, J. Anzai, *Langmuir* **2002**, 18, 7024.
- [45] M. L. Cortez, D. Pallarola, M. Ceolín, O. Azzaroni, F. Battaglini, *Chem. Commun.* **2012**, 48, 10868.
- [46] E. Piccinini, D. Pallarola, F. Battaglini, O. Azzaroni, *Chem. Commun.* **2015**, 51, 14754.
- [47] E. Piccinini, D. Pallarola, F. Battaglini, O. Azzaroni, *Mol. Syst. Eng.* **2016**, 1, 155.
- [48] S. Garreau, G. Louarn, J. P. Buisson, G. Froyer, S. Lefrant, *Macromolecules* **1999**, 32, 6807.
- [49] A. Schaarschmidt, A. A. Farah, A. Aby, A. S. Helmy, *J. Phys. Chem. B* **2009**, 113, 9352.
- [50] W. A. Marmisollé, J. Irigoyen, D. Gregurec, S. Moya, O. Azzaroni, *Adv. Funct. Mater.* **2015**, 25, 4144.
- [51] X. Song, Y. Ma, C. Wang, P. M. Dietrich, W. E. S. Unger, Y. Luo, *J. Phys. Chem. C* **2012**, 116, 12649.
- [52] W. A. Marmisollé, E. Maza, S. Moya, O. Azzaroni, *Electrochim. Acta* **2016**, 210, 435.
- [53] S. K. Jönsson, J. Birgersson, X. Crispin, G. Greczynski, W. Osikowicz, A. Denier van der Gon, W. Salaneck, M. Fahlman, *Synth. Met.* **2003**, 139, 1.
- [54] K. Svennersten, M. H. Bolin, E. W. H. Jager, M. Berggren, A. Richter-Dahlfors, *Biomaterials* **2009**, 30, 6257.
- [55] F. Arduini, F. D. Giorgio, A. Amine, F. Cataldo, D. Moscone, G. Palleschi, *Anal. Lett.* **2010**, 43, 1688.
- [56] A. J. Bard, L. R. Faulkner, *Electrochemical Methods: Fundamentals and Applications*, Wiley, New York **2001**.
- [57] D. Cheng, F. Shang, J. Ratner, *Bioconjugate Chem.* **2012**, 100, 130.
- [58] H. Wang, F. Cheng, M. Li, W. Peng, J. Qu, *Langmuir* **2015**, 31, 3413.
- [59] A. Lancuski, F. Bossard, S. Fort, *Biomacromolecules* **2013**, 14, 1877.
- [60] A. Baba, J. Lübben, K. Tamada, W. Knoll, *Langmuir* **2003**, 9058.
- [61] I. Willner, S. Rubin, Y. Cohen, *J. Am. Chem. Soc.* **1993**, 113, 4937.
- [62] D. Pallarola, N. Queralto, F. Battaglini, O. Azzaroni, *Phys. Chem. Chem. Phys.* **2010**, 12, 8071.
- [63] K. Prime, G. Whitesides, *Science* **1991**, 252, 1164.
- [64] E. Ostuni, R. G. Chapman, R. E. Holmlin, S. Takayama, G. M. Whitesides, *Langmuir* **2001**, 17, 5605.
- [65] M. Hederes, P. Konradsson, B. Liedberg, *Langmuir* **2005**, 21, 2971.
- [66] A. Yu, J. Shang, F. Cheng, B. A. Paik, J. M. Kaplan, R. B. Andrade, D. M. Ratner, *Langmuir* **2012**, 28, 11265.
- [67] *Bioelectronics: From Theory to Applications* (Ed: I. Willner), WILEY-VCH, Weinheim **2005**.
- [68] C. Bourdillon, C. Demaille, J. Moiroux, J.-M. Savéant, *Acc. Chem. Res.* **1996**, 29, 529.
- [69] *Protein Architecture: Interfacing Molecular Assemblies and Immobilization Biotechnology* (Eds: Y. Lvov, H. Möhwald), Marcel Dekker, New York **2000**.
- [70] C. Bourdillon, C. Demaille, J. Gueris, J. Moiroux, J. M. Saveant, *J. Am. Chem. Soc.* **1993**, 115, 12264.
- [71] B. Piro, L. A. Dang, M. C. Pham, S. Fabiano, C. Tran-Minh, *J. Electroanal. Chem.* **2001**, 512, 101.
- [72] K. Rechendorff, M. B. Hovgaard, M. Foss, V. P. Zhdanov, F. Besenbacher, *Langmuir* **2006**, 22, 10885.
- [73] E. Piccinini, C. Bliem, C. Reiner-Rozman, F. Battaglini, O. Azzaroni, W. Knoll, *Biosens. Bioelectron.* **2017**, 92, 661.
- [74] X. Xiao, M. Wang, H. Li, P. Si, *Talanta* **2013**, 116, 1054.
- [75] S. Fabiano, C. Tran-Minh, B. Piro, L. A. Dang, M. C. Pham, O. Vittori, *Mater. Sci. Eng., C* **2002**, 21, 61.
- [76] P.-C. Nien, T.-S. Tung, K.-C. Ho, *Electroanalysis* **2006**, 18, 1408.
- [77] J.-Y. Chiu, C.-M. Yu, M.-J. Yen, L.-C. Chen, *Biosens. Bioelectron.* **2009**, 24, 2015.
- [78] A. Wisitsoraat, S. Pakapongpan, C. Sriprachubwong, D. Phokharatkul, P. Sritongkham, T. Lomas, A. Tuantranont, *J. Electroanal. Chem.* **2013**, 704, 208.
- [79] J. Park, H. K. Kim, Y. Son, *Sens. Actuators, B* **2008**, 133, 244.
- [80] F. Ma, A. Rehman, H. Liu, J. Zhang, S. Zhu, X. Zeng, *Anal. Chem.* **2015**, 87, 1560.
- [81] A. Williamson, M. Ferro, P. Leleux, E. Ismailova, A. Kaszas, T. Doublet, P. Quilichini, J. Rivnay, B. Rózsa, G. Katona, C. Bernard, G. G. Malliaras, *Adv. Mater.* **2015**, 27, 4405.
- [82] B. Winther-Jensen, D. W. Breiby, K. West, *Synth. Met.* **2005**, 152, 1.
- [83] S. T. Larsen, R. F. Vreeland, M. L. Heien, R. Taboryski, *Analyst* **2012**, 137, 1831.
- [84] T. Hatakeyama, K. Murakami, Y. Miyamoto, N. Yamasaki, *Anal. Biochem.* **1996**, 237, 188.
- [85] H. Haas, H. Möhwald, *Thin Solid Films* **1989**, 180, 101.
- [86] T. Y. Kim, J. E. Kim, K. S. Suh, *Polym. Int.* **2006**, 55, 80.
- [87] W. Knoll, *Annu. Rev. Phys. Chem.* **1998**, 49,
- [88] E. S. Forzani, M. Otero, M. A. Pérez, M. L. Teijelo, E. J. Calvo, *Langmuir* **2002**, 18, 4020.
- [89] H. Zhao, P. H. Brown, P. Schuck, *Biophys. J.* **2011**, 100, 2309.
- [90] H. Ai, X. Huang, Z. Zhu, J. Liu, Q. Chi, Y. Li, Z. Li, X. Ji, *Biosens. Bioelectron.* **2008**, 24, 1048.